

Black hole growths in gamma-ray bursts driven by the Blandford-Znajek mechanism

Xiao-Yan Li, and Tong Liu^{*}

Department of Astronomy, Xiamen University, Xiamen, Fujian 361005, China

Accepted XXX. Received YYY; in original form ZZZ

ABSTRACT

The Blandford-Znajek (BZ) mechanism in stellar-mass black hole (BH) hyperaccretion systems is generally considered to power gamma-ray bursts (GRBs). Based on observational GRB data, we use the BZ mechanism driven by the BH hyperaccretion disc to investigate the evolution of the BH mass and spin after the jets break out from the progenitors. We find that the BH growths are almost independent of initial BH masses. Meanwhile, the BH growths will be more efficient with smaller initial spin parameters. We conclude that (i) the BZ mechanism is efficient for triggering BH growths for only 1 of 206 typical long-duration GRBs; (ii) the mean BH mass growths of ultra-long GRBs are marginal for all 7 samples collected; (iii) for the short-duration GRBs, the results that BHs show minimal growths is consistent with the mass supply limitation in the scenario of compact object mergers.

Key words: accretion, accretion discs - black hole physics - gamma-ray burst: general - magnetic fields

1 INTRODUCTION

Gamma-ray bursts (GRBs) are the most luminous transients associated with gravitational waves, neutrinos, and cosmic rays known in the universe. Based on the GRB prompt duration T_{90} , defined as the interval when 5%-95% of the burst fluence is accumulated, GRBs are classified as long-duration GRBs (LGRBs; $T_{90} > 2$ s) and short-duration GRBs (SGRBs; $T_{90} < 2$ s) (e.g., Kouveliotou et al. 1993) or Type I and II GRBs (e.g., Zhang 2006; Zhang et al. 2007a). Some LGRBs are confirmed to be associated with Type Ib/c supernovae (SNe, see e.g., Hjorth et al. 2003; Stanek et al. 2003; Malesani et al. 2004; Berger et al. 2011). The association of some LGRBs with SNe suggests that LGRBs originated from the collapses of massive stars ($> 8 M_{\odot}$, e.g., Woosley 1993; Paczyński 1998). SGRBs are generally believed relevant to the mergers of compact objects, i.e., a binary neutron star (NS) or black hole (BH)-NS (e.g., Eichler et al. 1989; Narayan, Paczyński, & Piran 1992; Nakar 2007). Interestingly, ultra-long GRBs (ULGRBs; $T_{90} > 1000$ s) have been observed in the past decade (e.g., Gendre et al. 2013; Levan et al. 2014). Some literatures proposed that ULGRBs may belong to the third population and have novel progenitors (e.g., Levan et al. 2014; Greiner et al. 2015). On the other hand, the lack of compelling evidences prevents a new classification in the burst-duration distribution (e.g., Virgili et al. 2013; Zhang et al.

2014). In addition, ULGRBs are associated with SNe, which implies that they might be produced by the massive collapsars (e.g., Greiner et al. 2015; Liu et al. 2018).

For both collapse and merger scenarios, a rotating BH surrounded by a hyperaccretion disc (e.g., Paczyński 1991; MacFadyen & Woosley 1999; Liu, Gu, & Zhang 2017) or a magnetar (e.g., Duncan & Thompson 1992; Usov 1992; Dai & Lu 1998a,b; Metzger et al. 2011) can be formed. In the hyperaccretion system, the violent accretion powers an energetic engine, then the neutrino annihilation processes (e.g., Ruffert et al. 1997; Popham, Woosley, & Fryer 1999; Rosswog, Ramirez-Ruiz, & Davies 2003; Liu et al. 2007; Zalamea & Beloborodov 2011; Kawanaka, Piran, & Krolik 2013) or the Blandford-Znajek (BZ) mechanism (e.g., Blandford & Znajek 1977; Lee, Wijers, & Brown 2000; Liu et al. 2015a) can produce the ultrarelativistic jets to trigger GRBs (for a review, see Liu, Gu, & Zhang 2017). A neutrino-dominated accretion flow (NDAF) around a stellar-mass BH with an extremely high accretion rate is a plausible candidate for the central engine. In this scenario, neutrinos exploit the thermal energy of the heated disc and liberate enormous binding energy, and then annihilate outside of the disc to produce the fireball. The BZ mechanism is an alternative model to drive GRB jets, in which case the BH's rotational energy are efficiently extracted by the Poynting jets.

Moreover, the evolution of BH mass and spin may be violent in the hyperaccretion system (e.g., Liu et al. 2015b; Song et al. 2015; Qu & Liu 2022). If the initial BH mass

^{*} E-mail: tongliu@xmu.edu.cn

is set as to approximately $3 M_{\odot}$, according to the neutrino annihilation process, the final BH mass is relatively large ($> 5 M_{\odot}$) for LGRBs and small ($3 - 5 M_{\odot}$) for SGRBs. The BZ mechanism is less efficient in triggering BH growths compared with the neutrino annihilation processes (e.g., Liu et al. 2015a; Qu & Liu 2022). However, in the scenarios of massive collapsars and compact object mergers, the neutrino annihilation process could only last for several or tens of seconds until the ignition accretion cannot be reached with the decreasing accretion rate. Then it might be quickly replaced by the BZ mechanism and jets could break out from the envelopes or ejecta, especially for collapsar model (e.g., Liu et al. 2018; Wei, Liu, & Xue 2021). Moreover, the typical luminosity of the neutrino annihilation process is lower than that of the BZ mechanism by about two orders of magnitude with the same high spin parameter and accretion rate (e.g., Liu et al. 2015a). If the disc outflows are considered, the above conclusion will be strengthened. Of course, one cannot rule out that the neutrino annihilation process will be dominated in the activities of GRB central engines (e.g., Liu, Gu, & Zhang 2017). Here we generally discussed the BH growths of GRBs powered by the BZ mechanism and set the initial BH properties at the moment that the jets break out from the envelopes of the massive collapsars or the ejecta of the compact object mergers. The growth caused by the BZ mechanism is small but not totally negligible, which is directly related to the observable GRBs as mentioned above. The growths of the BHs in the center of GRBs is an inevitable course in the evolution history of stellar-mass BHs, then effects the mass distribution of compact objects (e.g., Liu et al. 2021).

In this paper, combining with the GRB samples, we visit the BH hyperaccretion system with the BZ mechanism to test the suitability of the BZ mechanism for GRBs and investigate the growths of newborn BHs in the center of GRBs. This paper is organised as follows. In Section 2, the model for the evolution of BH characteristic parameters is described. The results are shown in Section 3. Conclusions and discussion are presented in Section 4.

2 MODEL

The characteristic parameters of the BH will undergo drastic evolution if a rotating stellar BH surrounded by a hyperaccretion disc with a very high accretion rate is the central engine of GRBs (e.g., Liu et al. 2015b; Song et al. 2015; Qu & Liu 2022). Based on the conservation of the mass and angular momentum, considering that part of the BH rotational energy would be extracted by the Poynting jet for the BZ mechanism, the mass and angular momentum of a Kerr BH evolved with time read as (e.g., Lee, Wijers, & Brown 2000; Lee & Kim 2000)

$$\frac{dM_{\text{BH}}}{dt} = \dot{M}e_{\text{ms}} - \frac{L_{\text{BZ}}}{c^2}, \quad (1)$$

$$\frac{dJ_{\text{BH}}}{dt} = \dot{M}l_{\text{ms}} - \frac{L_{\text{BZ}}}{c^2\Omega_{\text{F}}}, \quad (2)$$

where M_{BH} and J_{BH} are the mass and angular momentum of the BH, \dot{M} is the mass accretion rate, c is the speed of light, and e_{ms} and l_{ms} are the specific energy and

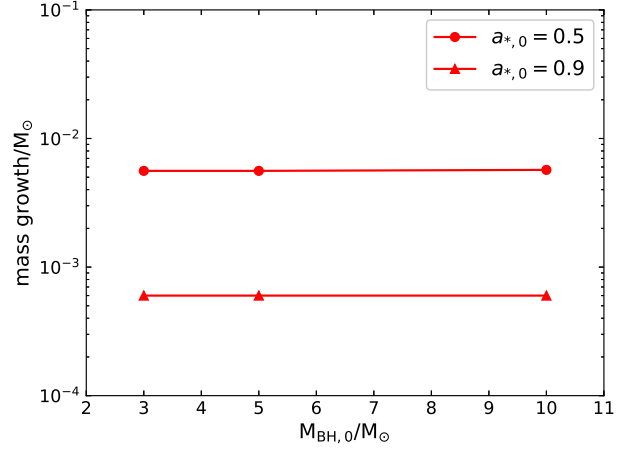


Figure 1. Influence of initial BH masses and spin parameters on BH mass growths in a typical GRB case with the luminosity $L_j = 10^{49} \text{ erg s}^{-1}$ and duration $T_{90} = 30 \text{ s}$. The circles and triangles represent the initial BH spin $a_{*,0} = 0.5$ and 0.9 , respectively.

angular momentum corresponding to the marginally stable orbit radius of the BH. They are defined as $e_{\text{ms}} = \frac{1}{\sqrt{3x_{\text{ms}}}} \left(4 - \frac{3a_*}{\sqrt{x_{\text{ms}}}} \right)$ and $l_{\text{ms}} = 2\sqrt{3} \frac{GM_{\text{BH}}}{c} \left(1 - \frac{2a_*}{3\sqrt{x_{\text{ms}}}} \right)$, where $a_* \equiv cJ_{\text{BH}}/GM_{\text{BH}}^2$ ($0 \leq a_* \leq 1$) is the dimensionless spin parameter of the BH and x_{ms} is the dimensionless marginally stable orbit radius of the BH, which can be written as $x_{\text{ms}} = 3 + Z_2 - \sqrt{(3 - Z_1)(3 + Z_1 + 2Z_2)}$ with $Z_1 = 1 + (1 - a_*^2)^{1/3}[(1 + a_*)^{1/3} + (1 - a_*)^{1/3}]$ and $Z_2 = \sqrt{3a_*^2 + Z_1^2}$ (e.g., Bardeen, Press, & Teukolsky 1972; Novikov 1998; Kato, Fukue, & Mineshige 2008). The last two terms on the right-hand side of Equations (1) and (2) are relevant to the BZ mechanism, where L_{BZ} is the BZ jet power and Ω_{F} is the magnetic field angular velocity at the marginally stable orbit radius. Here, we adopt the optimal mode $\Omega_{\text{F}} = \Omega_{\text{H}}/2$ (e.g., Lee, Wijers, & Brown 2000; Lee & Kim 2000), with $\Omega_{\text{H}} \equiv a_* c^3/[2(1 + \sqrt{1 - a_*^2})GM_{\text{BH}}]$ being the angular velocity on the stretched horizon.

The mean luminosity of the GRB jet can be estimated as (e.g., Fan & Wei 2011; Liu et al. 2015b)

$$L_j \simeq \frac{(E_{\gamma,\text{iso}} + E_{\text{k,iso}})(1+z)\theta_j^2}{2T_{90}}, \quad (3)$$

where $E_{\gamma,\text{iso}}$ is the isotropic radiated energy in the prompt emission phase, $E_{\text{k,iso}}$ is the isotropic kinetic energy powering long-lasting afterglow, z is the redshift, θ_j is the half-opening angle of the jet, and T_{90} can be approximately considered as the duration of the violent activity of the central engine for both LGRBs and SGRBs. Using these observational GRB data, the jet luminosity L_j can be obtained. From the data of the prompt emission and afterglows, one can obtain the value of $E_{\gamma,\text{iso}}$ and $E_{\text{k,iso}}$, and the radiative efficiency in the fireball model is implied in the fitting process. Generally, $E_{\text{k,iso}}$ is larger than $E_{\gamma,\text{iso}}$ in most of cases as shown in Tables 1, 2, and 3. Moreover, in fireball model (e.g., Rees & Mészáros 1992; Mészáros & Rees 1993), the energy is released by the central engine in a very short timescale. The collisions of the shells in the internal shock phase will trigger the prompt emission and the ex-

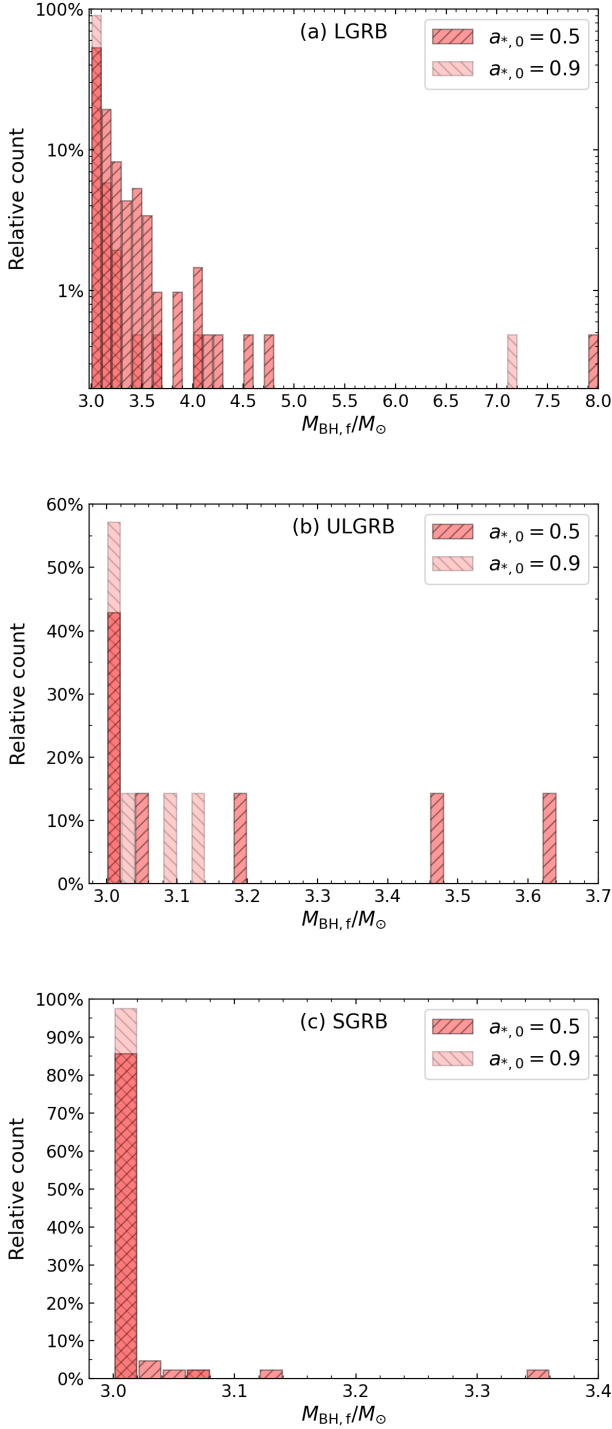


Figure 2. Distributions of the final BH masses $M_{\text{BH},f}$. The initial BH mass $M_{\text{BH},0}$ is $3 M_{\odot}$. The dark and light colors denote $a_{*,0} = 0.5$ and 0.9 , respectively.

ternal shocks sweeping the circumstellar media will power the long-lasting multiband afterglows. T_{90} is considered to reflect the activity timescale of the GRB central engines.

For a BH hyperaccretion system in the centre of GRBs with the BZ mechanism, the energy output is determined by the BZ jet power L_{BZ} . It is related to the BH mass accre-

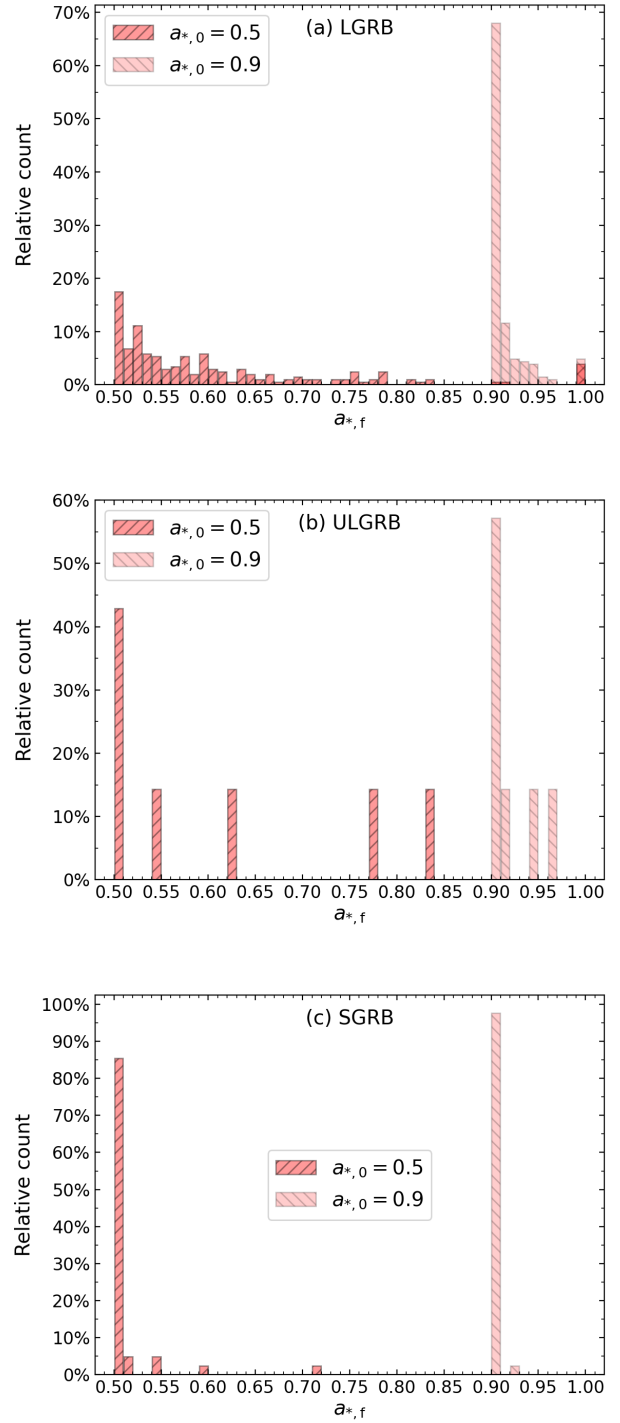


Figure 3. Distributions of the final BH spin parameters $a_{*,f}$. The dark and light colors denote $a_{*,0} = 0.5$ and 0.9 , respectively.

tion rate and the spin parameter a_* , which writes as (e.g., Liu et al. 2018; Du et al. 2021)

$$L_{\text{BZ}} = 9.3 \times 10^{53} a_*^2 \dot{m} X(a_*) \text{ erg s}^{-1}, \quad (4)$$

where $X(a_*) = F(a_*) / (1 + \sqrt{1 - a_*^2})^2$, with $F(a_*) = [(1 + q^2) / q^2] [(q + 1/q) \arctan(q) - 1]$ and $q = a_* / (1 +$

$\sqrt{1 - a_*^2}$. Parameters $m_{\text{BH}} = M_{\text{BH}}/M_{\odot}$ and $\dot{m} = \dot{M}/M_{\odot} \text{ s}^{-1}$ are introduced in this work.

If we assume $L_j = L_{\text{BZ}}$, the dimensionless mass accretion rate can be obtained as the function of L_j :

$$\dot{m} = \frac{L_j}{9.3 \times 10^{53} a_*^2 X(a_*) \text{ erg s}^{-1}}. \quad (5)$$

According to the above equations, the final BH characteristics can be described. With a given initial BH mass (e.g. $M_{\text{BH},0} = 3 M_{\odot}$) and spin ($a_{*,0} = 0.5$ and 0.9) and the luminosity of a GRB jet L_j obtained by Equation (3), one can obtain the BZ jet power L_{BZ} and the values of \dot{m} based on Equations (4) and (5), respectively. Incorporating \dot{m} and L_{BZ} into the Equations (1) and (2), the mass and spin of the BH at the next time step can be solved. Step by step, the final BH mass $M_{\text{BH},f}$ and spin $a_{*,f}$ can be obtained when the time reaches T_{90} . The fourth-order Runge-Kutta method, ode45 function of MATLAB, is used in our calculations. The main results are discussed below.

3 RESULTS

In this work, we adopt the data of 206 LGRBs, 7 ULGRBs, and 41 SGRBs to calculate the evolution of BH mass and spin in the BH hyperaccretion system with the BZ mechanism. The duration T_{90} , redshifts z , half-opening angles θ_j , and isotropic radiated energy in the prompt emission phase $E_{\gamma,\text{iso}}$ and isotropic kinetic energy $E_{k,\text{iso}}$ of the LGRBs, ULGRBs and SGRBs are collected in Tables 1, 2, and 3, respectively. The GRBs associated with SNe are labelled by the superscript “*”. The GRB luminosity derived from Equation (3) is also presented. It should be noticed that the measurements of $E_{\gamma,\text{iso}}$ and $E_{k,\text{iso}}$ are model dependent. Besides, the lower limits of θ_j are used in some bursts.

Before the discussion of the GRB cases collected, theoretical results of mass growths with different initial BH masses and spin parameters are illustrated in Figure 1 based on our model. In the figure, we adopt a typical GRB luminosity $L_j = 10^{49} \text{ erg s}^{-1}$ and duration $T_{90} = 30 \text{ s}$ to calculate the BH mass growths with different initial BH masses, i.e., 3, 5, and $10 M_{\odot}$ and different initial spin parameters, i.e., $a_{*,0} = 0.5$ and 0.9 . One can find that the final BH mass is almost independent of the initial BH mass ($\leq 10 M_{\odot}$) but depend on the initial spin and the BH growth will be more efficient with a smaller spin parameter. The conclusion can also be directly inferred from Equation (5). For a given luminosity, the initial BH mass has no effect on the accretion rate and then on the mass growth. However, the accretion rate is relevant to the BH spin, the larger initial spin parameter leads to a lower accretion rate, and thus a less final mass. As shown in Figure 1, one can see that the mass growth is about $6 \times 10^{-3} M_{\odot}$ even with $a_{*,0} = 0.5$. There is almost no change for the evolution of BH mass with the BZ mechanism for the typical luminosity and duration, and thus one can expect that the BH growths will be obvious only for the case with high GRB luminosity and long accretion timescale.

The BH mass before accretion might be around $3 M_{\odot}$ for the scenarios of the collapsars or the compact object mergers (e.g., Abbott et al. 2017, 2021; Belczynski et al. 2008; Liu et al. 2021; Wei, Liu, & Xue 2021; Qu & Liu 2022). In the collapsar scenario, if the NDAF phase lasts several to tens of seconds, the central BH should be fed to grow

up, but the disc outflows will decrease the BH’s appetite, and more important, the jets might be choked in the envelope and no observable electromagnetic signals. For merger scenarios, the jet may also be choked by the tidal and/or post-merger ejecta (e.g., Murguia-Berthier et al. 2021). Considering the dissipative energy by the choked jets to build cocoon, the total GRB energy should be less than the real released energy and the BH mass growth will be more violent. Here we just investigate the BH evolution after the jets break out from the progenitors. Combining with the result that the initial BH mass has almost no effect on the mass growths as shown in Figure 1, we use $M_{\text{BH},0} = 3 M_{\odot}$ in the GRBs sample calculations. Besides, $a_{*,0} = 0.5$ and 0.9 are adopted.

3.1 LGRB case

The distributions of final BH masses $M_{\text{BH},f}$ and spins $a_{*,f}$ for LGRB cases are presented in Figures 2(a) and 3(a), respectively. The dark and light colors denote the initial BH spins $a_{*,0} = 0.5$ and 0.9 . As mentioned above, the mass growth under the BZ mechanism is inefficient. Thus, high GRB luminosity and long accretion timescale are required in this case. Moreover, a smaller initial BH spin parameter is favored.

Figure 2(a) shows the final BH masses distribution after the accretion phase for 206 LGRB events. If the initial BH mass $M_{\text{BH},0}$ is $3 M_{\odot}$, the mean final BH masses are about $3.203 M_{\odot}$ for $a_{*,0} = 0.5$ and $3.059 M_{\odot}$ for $a_{*,0} = 0.9$. One can find that a smaller $a_{*,0}$ leads to a higher $M_{\text{BH},f}$ and that most of the final BH masses are below $5 M_{\odot}$. With relatively high jet luminosity and long accretion time, one bursts, namely, GRB 050401, has a final BH mass larger than $5 M_{\odot}$, which are $7.992 M_{\odot}$ for $a_{*,0} = 0.5$ and $7.172 M_{\odot}$ for $a_{*,0} = 0.9$, respectively, for which the BZ mechanism is a plausible prescription.

In Figure 3(a), we show the distribution of the final BH spins for the LGRB events. The mean final BH spin parameters are about 0.60 for $a_{*,0} = 0.5$ and 0.91 for $a_{*,0} = 0.9$. The upper limit of the BH spin is set as 0.998 (e.g., Kato, Fukue, & Mineshige 2008). The bursts with larger final BH masses have higher final BH spin parameters, and several bursts including the GRB 050401 mentioned above, can reach up to the spin limitation.

In our calculation GRB 050401 is a special case with high luminosity, which is mainly caused by the relatively high kinetic energy. Actually, some other bursts have the similar or even higher kinetic energy but with lower luminosity because of other parameters, such as the opening angle and T_{90} . Besides, it should be mentioned that the fitting of the kinetic energy is model-dependent (e.g., Zhang et al. 2007b). We noticed that Kamble et al. (2009) used a double-jet model to fit the X-ray afterglow of GRB 050401, the kinetic energies of the narrow and wide jets are $\sim 5.46 \times 10^{53} \text{ erg}$ and $> 5.07 \times 10^{51} \text{ erg}$, respectively, which are much less than the value adopted here.

It is widely accepted that LGRBs signal the collapse of massive stars, which usually end their lives accompanied with SNe. The conclusion is confirmed by the observation evidence, such as the appearance of SN-like bumps in the optical afterglow light curves of several bursts (e.g., Hjorth et al. 2003; Zhang et al. 2009). There is competition on the lumi-

nosity of LGRBs and those of corresponding SN bumps (e.g., Song & Liu 2019; Liu et al. 2021). Thus, the typical luminosity of LGRBs associated with SNe is lower than that of LGRBs without observable SNe, which will further decrease the values of the BH growths. We indeed find that the BH growths are less obviously for LGRBs associated with SNe in most cases. Besides, it should be noticed that the SN explosions may exist in the cases without SNe observed in result of that they are too weak (even failed) or too distant to be observed.

3.2 ULGRB case

ULGRBs are characterised by gamma-ray emission lasting longer than ~ 1000 s. Although their duration are different as typical LGRBs, the evidence for a new GRB classification is still unclear (e.g., Zhang et al. 2014; Perna, Lazzati, & Cantiello 2018). Even so, given by the long accretion time, we expect correspondingly large BH growths and we thus separate them in Table 2.

The distribution of the final BH masses after the accretion phase for ULGRB events is shown in Figure 2(b). The figure shows that the mass growths are marginal. None of the bursts in the sample has a final BH mass larger than $5 M_{\odot}$ even with $a_{*,0} = 0.5$ for the initial BH mass $M_{\text{BH},0} = 3M_{\odot}$. In this case, the mean final BH masses are about $3.193 M_{\odot}$ and $3.039 M_{\odot}$ for $a_{*,0} = 0.5$ and 0.9 , respectively.

Figure 3(b) presents the distribution of the final BH spins for ULGRB events. The evolution of spin parameters is also inefficient. The mean final BH spin parameters are about 0.61 for $a_{*,0} = 0.5$ and 0.92 for $a_{*,0} = 0.9$.

One can find that the BH growths are inefficient for ULGRBs. This is because the long accretion time cannot offset the effect caused by the low burst luminosity.

3.3 SGRB case

Similar to LGRBs, the evolution of BH characteristic parameters is investigated for SGRBs. For the merger scenario, the ejecta hardly stops the SGRB jets, but the limited accretion matter can only support the central engine activity for no more than seconds. Thus, one can expect that the growths of BHs in the centre of SGRBs are undoubtedly very limited.

The distributions of the final BH masses and spin parameters of 41 SGRB events are presented in Figures 2(c) and 3(c), respectively. We find that if the initial BH mass $M_{\text{BH},0} = 3M_{\odot}$, the mean final BH masses are about $3.0173 M_{\odot}$ for $a_{*,0} = 0.5$ and $3.0026 M_{\odot}$ for $a_{*,0} = 0.9$. Besides, the mean final BH spin parameters are about 0.512 for $a_{*,0} = 0.5$ and 0.901 for $a_{*,0} = 0.9$. It shows that the effect on the evolution of BH characteristic parameters is not significant and the final BH masses for all of the bursts are between $3\text{-}5 M_{\odot}$.

As the results, the BH growths in SGRBs is consistent with the mass supply limitation in the scenario of compact object mergers.

4 CONCLUSIONS AND DISCUSSION

Based on the observational data, we test the capacity of the BZ mechanism to power GRBs and present the growths of BHs in the center of GRBs. The BZ mechanism is capable of powering all types of GRBs with reasonable parameters of BH hyperaccretion systems and the main conclusions are summarised as follows:

(i) By assuming GRBs powered by the BZ jets, for LGRBs with typical durations, the mean BH mass growth is about $0.203 M_{\odot}$ for $a_{*,0} = 0.5$. Only GRB 050401 has a final BH mass larger than $5 M_{\odot}$ for the initial BH mass $\sim 3 M_{\odot}$. At the same time, the BH spin parameter for GRB 050401 almost reaches up to 0.998 .

(ii) For ULGRBs with duration $T_{90} > 1000$ s, the mean BH mass growth is about $0.193 M_{\odot}$ for $a_{*,0} = 0.5$.

(iii) For SGRBs, the mean BH mass growths are about $0.0173 M_{\odot}$ for $a_{*,0} = 0.5$ and $0.0026 M_{\odot}$ for $a_{*,0} = 0.9$.

It should be noticed that the jet half-opening angle θ_j is usually estimated by the jet break time in X-ray afterglows and it is hard to constrain since the absence of jet break observations. The lower limits of θ_j are widely used (e.g., Liu et al. 2015b; Yi et al. 2017), and therefore one can see from Equation (3) that the BH growths are lower limits in this work.

The assumption of a Keplerian disc is adopted in this work. Actually, Gammie, Shapiro, & McKinney (2004) investigated the BH spin evolution for the thick torus accretion, and they found that the spin-down effects will be resulted in case of large initial spins for some physical processes. Besides, Janiuk, Moderski, & Proga (2008) studied the evolution of the BH spin in LGRB cases and found that the spin-down of the BH is possible due to the low specific angular momentum of the accretion materials.

The Swift satellite observations have revealed the diverse morphology of light curves in X-ray afterglows (e.g., Gehrels et al. 2004; Burrows et al. 2005). Among them, X-ray flares are important signatures, which may be caused by the restart of central engine (e.g., Burrows et al. 2005; Liu, Gu, & Zhang 2017). The BZ mechanism is a promising candidate to explain the GRBs accompanied by long-lasting X-ray flares (e.g., Luo et al. 2013). If the effect of flares is considered, the evolution of BH will be more violent. In addition, the long-lasting plateau phases are observed in some GRB afterglows, and energy injection is one of the most widely accepted explanations (e.g., Fan & Xu 2006; Zhang et al. 2006). In this case, the external shock will be refreshed by the huge energy contribution from the central engine. As well as X-ray flares, if the plateau phase induced by the energy injection is originated from the long-lasting BH hyperaccretion (e.g., Huang & Liu 2021), the BH will undergo more drastic evolution to promote its growths.

Moreover, in collapsar and merger scenarios, the outflows from the BH hyperaccretion disc are definitely strong (e.g., Liu et al. 2018) and will inject matter and energy into the shock to power luminous SNe and kilonovae (e.g., Surman, McLaughlin, & Hix 2006; Song, Liu, & Li 2018; Song & Liu 2019; Metzger 2019; Qi et al. 2022). Once the disc outflows are strong enough, the accretion rate in the inner region of the disc is too low to ignite NDAFs, which

Table 1. LGRB data

GRB	z	T_{90} (s)	θ_j (rad)	$E_{\gamma, \text{iso}}$ (10^{52} erg)	$E_{k, \text{iso}}$ (10^{52} erg)	L_j (10^{49} erg s $^{-1}$)	Ref
970508	0.8349	14.0	0.3775	0.61	0.99	14.94	1
970828	0.96	160	0.1239	29	37.154	6.22	1
971214	3.418	31.23	>0.0967	21	8.48	19.50	1
980425*	0.01	23.3	0.192	0.000093	0.00631	0.01	2
980613	1.0964	42.0	>0.2194	0.59	1.22	2.17	1
980703	0.966	76.0	0.1957	7.2	2.41	4.76	1
990123	1.61	63.3	0.064	229	534	64.43	1
990510	1.619	67.58	0.0586	17	13.16	2.01	1
990705	0.84	32.0	0.093	18	0.34	4.56	1
991208	0.706	68	0.12	12	2.2	2.57	3
991216	1.02	15.17	0.0798	67	36.64	43.94	1
000210	0.846	9.0	>0.1194	14.9	0.5	22.52	1
000926	2.0387	1.30	0.1075	27.1	9.97	500.67	1
010222	1.4769	74.0	0.0559	81	22.79	5.43	1
011121*	0.362	47	0.157	7.8	2.7	3.75	2
011211	2.14	51.0	0.1114	5.4	71.32	29.31	1
020405	0.69	60	0.0822	14.79	945.48	91.38	4
020813	1.25	89	0.0541	66	204.174	10.00	1
021004	2.3304	77.1	0.2211	3.3	8.35	12.30	1
021211*	1	2.8	0.024~0.0768	1.12	4	1.09	2
030226	1.986	100	0.0417	7.94	2392.17	62.31	4
030323	3.37	26	0.0326	3.2	1093.91	97.99	4
030329*	0.17	22.3	0.089	1.33	6.31	1.59	2
031203*	0.1	40	0.157	0.0167	0.138	0.05	2
050126	1.29	30	0.365	0.8	39.8	206.44	1
050315	1.95	96	0.0759	5.7	512.403	45.86	1
050318	1.4436	32	0.038	2.2	11.259	0.74	1
050319	3.2425	139.4	0.038	4.6	77.896	1.81	1
050401	2.9	38	0.472	35	4570.9	52656.20	1
050416A	0.654	5.4	0.237	0.1	15.1	130.75	1
050505	4.27	63	0.029	16	237.829	8.93	1
050525A*	0.606	8.84	0.0551	2.5	8.2	2.95	2
050730	3.97	155	>0.023	9	86.1223	0.81	1
050802	1.71	20	0.290	1.8197	616.6	3523.62	1
050803	0.42	87.9	0.333	0.25	37.5	33.81	5
050814	5.3	48	0.0419	6	831.764	96.52	1
050820A	2.615	600	0.184	97.4	53.7145	15.41	1
050904	6.295	183.6	0.034	124	88.37	4.88	1
050922C	2.198	4.5	0.026	5.3	47.725	12.74	1
051022	0.8	200	0.03	44	33.6	0.31	3
051109A	2.35	360	0.0593	6.5	169.824	2.88	1
051109B	0.08	14.3	0.4194	0.000679	0.02	0.14	5
051111	1.55	47	0.018	10.99	81.6	0.81	4
060115	3.53	139.6	0.126	6.05	85.68	23.63	5
060124	2.297	298	0.0531	41	578.87	9.67	1
060206	4.05	5	0.0351	4.3	386.76	243.30	1
060210	3.91	220	0.024	42	1313.2261	8.71	1
060418	1.49	52	0.029	13	7.5307	0.41	1
060502A	1.51	28.4	0.3792	1.76	4.05	36.92	5
060505*	0.089	4	0.4	0.0012	0.028	0.64	1
060526	3.21	258.8	0.063	2.6	15.58	0.59	1
060604	2.1357	95	0.1188	0.26	29.57	6.95	5
060605	3.8	19	>0.046	2.5	115	31.41	1
060607A	3.082	100	>0.095	9	0.822	1.81	1
060614*	0.12	6.9	0.2025	0.21	1.698	6.35	1
060707	3.42	210	0.1379	5.4	102.329	21.56	1
060708	1.92	10.2	0.332	0.96	0.52	23.35	5
060714	2.71	108.2	0.0201	7.7	250.46	1.79	1
060729	0.54	115.3	0.4687	0.53	15.56	23.61	5
060814	1.9229	145.3	0.1748	6.09	32.66	11.91	5
060904B	0.703	192	>0.174	0.72	9.4031	1.36	6
060906	3.686	43.5	0.0684	9.13	28.23	9.41	5
060908	1.8836	18	0.008	9.8	2017.68	10.39	1
061007	1.262	75	>0.138	86	29.9425	33.30	1

Table 1 – continued

GRB	z	T_{90} (s)	θ_j (rad)	$E_{\gamma, \text{iso}}$ (10^{52} erg)	$E_{k, \text{iso}}$ (10^{52} erg)	L_j (10^{49} erg s $^{-1}$)	Ref
061021	0.35	79	0.1501	10	6.166	3.11	1
061110A	0.758	40.7	0.2532	0.44	0.38	1.14	5
061121	1.314	81	0.099	22.5	20.5215	6.02	1
061222A	2.09	16	0.0471	21	2290.868	495.24	1
070110	2.352	89	>0.274	3	0.687	5.21	1
070125	1.5477	63	0.2304	80.2	6.43	92.98	1
070129	2.3384	460.6	0.1422	8.06	42.92	3.74	5
070306	1.5	3	0.0768	6	67.608	180.90	1
070318	0.84	63	0.127	0.9	47.2719	11.35	1
070411	2.95	101	0.032	10	83.6596	1.88	1
070419A	0.97	112	>0.165	0.24	35.074	8.46	6
070508	0.82	23.4	0.0611	8	10.715	2.72	1
070529	2.4996	109.2	0.0996	4.7	17.06	3.46	5
071010A	0.98	6	0.09	0.13	7.2164	9.82	1
071010B	0.947	35.7	0.15	1.7	7.2713	5.50	1
071031	2.692	150.5	0.07	3.9	1.554	0.33	1
080109*	0.007	600	>0.1411	0.0000013	0.000446	0.0000075	7
080129	4.394	48	>0.097	7	29.138	19.11	6
080310	2.43	32	0.0628	6.0256	29.512	7.51	1
080319C	1.95	29.55	>0.102	14.1	74.4078	45.96	1
080330	1.51	61	>0.087	0.21	21.0923	3.32	1
080413B	1.1	8	0.1047	2.4	138.038	202.06	1
080430	0.767	16.2	0.2842	0.45	8.37	38.85	5
080516	3.2	5.8	0.0364	0.98	35.5	17.50	5
080603A	1.688	150	0.071	2.2	52.5129	2.47	1
080605	1.6398	20	0.0968	11.88	6.9	11.61	5
080707	1.23	27.1	0.1328	0.33	1.64	1.43	5
080710	0.845	120	>0.062	0.8	2.6451	0.10	1
080721	2.591	16.2	0.1252	69.31	78.49	256.78	5
080810	3.35	108	>0.105	45	41.8519	19.28	1
080905B	2.374	128	0.1318	5.76	16.44	5.08	5
080913	6.695	8	0.359	8.6	10	1152.90	1
081007*	0.53	9.01	>0.349	0.15	0.15	3.10	2
081008	1.967	162.2	0.0227	9.98	134.7	0.68	1
081203A	2.1	223	>0.116	35	11.2261	4.32	1
081221	2.26	34	0.118	34.3	8.03	28.26	5
081222	2.77	5.8	0.0489	30	131.826	125.76	1
090313	3.375	78	>0.093	3.2	276.8523	67.93	1
090323	3.568	133.1	0.0489	410	116	21.58	1
090328	0.7354	57	0.0733	13	82	7.77	1
090407	1.4485	310	0.0964	0.94	690	25.36	5
090418A	1.608	56	0.0881	17.06	12.57	5.36	5
090423*	8.23	10.3	0.0262	11	340	107.96	1
090424	0.544	49.47	>0.378	4.6	53.1215	128.71	1
090516	4.109	210	0.0762	69.02	75.01	10.17	5
090529	2.625	100	0.0981	1.41	91.37	16.18	5
090530	1.266	48	0.1795	0.68	3.19	2.94	5
090618	0.54	113.2	0.2817	13.39	12.72	14.09	5
090812	2.452	75.9	>0.071	40.3	148.827	21.68	1
090902B	1.8829	19.328	0.0681	1.77	56	19.98	1
090926A	2.1062	20	0.1571	210	6.8	415.51	1
091018	0.97	106.5	0.082	0.5888	12.023	0.78	1
091020	1.71	65	0.1204	12.2	51.286	19.18	1
091029	2.752	39.2	>0.192	7.4	40.303	84.16	1
091127*	0.48	68.7	0.096	4.3	22.9	2.70	2
091208B	1.063	71	0.1274	2.01	50.119	12.29	1
100418A	0.6235	8	0.356	0.99	3.36	55.94	1
100425A	1.755	37	0.1565	0.49	1.32	1.65	5
100615A	1.398	39	0.0791	5.82	16.66	4.32	5
100621A	0.542	63.6	>0.234	4.37	111.7596	77.09	1
100704A	3.6	197.5	0.1159	17.75	29.45	7.38	5
100728B	2.106	12.1	>0.063	2.66	95.665	50.09	1
100814A	1.44	174.5	0.1338	15.01	6160	772.88	5
100901A	1.408	439	0.152	6.3	167.3233	11.00	1
100906A	1.727	114.4	0.055	28.9	23.8173	1.90	1

Table 1 – *continued*

GRB	z	T_{90} (s)	θ_j (rad)	$E_{\gamma,iso}$ (10^{52} erg)	$E_{k,iso}$ (10^{52} erg)	L_j (10^{49} erg s $^{-1}$)	Ref
101219B*	0.552	51	>0.298	0.34	6.4	9.11	2
110205A	2.22	257	0.064	56	31.2172	2.24	1
110213A	1.46	48	>0.142	6.9	25.7527	16.87	1
110715A	0.82	13	0.2146	2.79	1.81	14.83	5
110808A	1.35	48	0.1894	17.86	0.88	16.46	5
111008A	4.9898	63.46	0.1059	42.11	23.77	34.87	5
111123A	3.1516	290	0.0544	23.78	89.24	2.39	5
111215A	2.06	374	0.03	14	770	2.89	3
111228A	0.714	101.2	0.259	4.17	13.89	10.26	5
120119A	1.728	70	0.032	36	4.17	0.80	1
120326A	1.798	11.8	0.0803	3.2	14	13.15	1
120327A	2.813	62.9	0.0694	8.78	8.45	2.52	5
120404A	2.876	48	>0.024	9	7.8	0.39	6
120422A*	0.283	5.35	0.2	0.0045	0.12	0.60	2
120521C	6	26.7	0.0524	8.25	22	10.89	1
120712A	4.1745	14.7	0.0467	18.57	8.69	10.46	5
120729A	0.8	72	0.0204	1.24	716.77	3.74	4
120811C	2.671	26.8	0.0486	6.96	27.8	5.62	5
120815A	2.358	9.7	>0.063	2.12	7.08	6.32	6
120922A	3.1	173	0.0977	21.38	59.62	9.16	5
120923A	8.1	26.1	0.0855	4.8	0.29	6.49	8
121024A	2.298	69	0.0741	1.84	32.61	4.52	5
121128A	2.2	23.3	0.0524	1.05	14.73	2.98	5
121211A	1.023	182	0.1026	0.17	37.76	2.22	5
130215A*	0.597	66	>0.1772	3.1	12.3	5.85	7
130420A	1.297	123.5	0.2103	0.23	3.72	1.62	5
130427A*	0.34	163	>0.0873	96	13.1	3.42	2
130606A	5.913	276.58	0.0498	21.67	86.86	3.36	5
130612A	2.006	4	0.0547	0.76	3.19	4.44	5
130702A*	0.145	59	0.086	0.064	37.7	2.71	2
130831A*	0.479	32.5	\geq 0.123	0.46	11.4	4.08	2
130907A	1.238	364	0.01	8	441	0.14	3
131030A	1.295	41.1	0.2149	17.22	6.73	30.88	5
131105A	1.686	112.3	0.1284	34.31	22.24	11.15	5
140206A	2.73	93.6	0.1291	30.68	46.28	25.56	5
140311A	4.954	70	0.03	10	2270	87.27	3
140423A	3.26	134	>0.3	65.4	2140	3155.04	9
140512A	0.725	154.8	0.093	9.07	51.44	2.92	5
140518A	4.707	60.5	0.0277	4.99	8.41	0.48	5
140606B*	0.384	23.6	0.14	0.347	0.039	0.22	2
140629A	2.276	42	0.04	4.4	1800	112.59	10
140703A	3.14	67.1	0.0285	1.95	1260	31.62	5
140903A	0.351	0.3	0.03	0.006	47.3	95.87	3
141121A	1.47	549.9	0.0635	0.02	54200	490.83	5
150403A	2.06	40.9	0.1101	1.51	248.8	113.51	5
150910A	1.359	112.2	0.0546	2.06	875	27.49	5
151027A	0.81	129.69	0.1562	3.38	28.71	5.46	5
151215A	2.59	17.8	0.0972	0.55	1.16	1.63	5
160121A	1.96	12	0.0331	0.77	208	28.21	5
160131A	0.97	325	0.0524	83	50	1.11	11
160227A	2.38	316.5	0.1711	4.06	12.76	2.63	5
160327A	4.99	28	0.0357	8.9	10.38	2.63	5
160509A	1.17	371	0.04	86	76.5	0.76	3
160625B	1.406	460	0.041	300	194	2.17	3
161108A	1.159	105.1	0.206	0.54	0.66	0.52	5
161117A	1.549	125.7	0.1525	23.29	42.15	15.43	5
161219B*	0.1475	10	0.6981	0.0097	0.016	0.72	7
170113A	1.968	20.66	0.1501	0.63	8.07	14.08	5
171010A	0.33	104	0.06	22	10.5	0.75	3
181110A	1.505	138.4	0.065	13.43	166	6.86	12
181201A	0.45	19.2	\gtrsim 0.1047	12	22	14.07	13
190106A	1.861	76.8	0.0733	10	9	1.90	14
190114C	0.425	116.354	>0.5672	41.2	190	455.47	15
190530A	0.9386	20.31	0.0665	143	3715.4	814.33	16
190829A	0.0785	57	0.015	27	40	0.14	17

Table 1 – continued

GRB	z	T_{90} (s)	θ_j (rad)	$E_{\gamma,iso}$ (10^{52} erg)	$E_{k,iso}$ (10^{52} erg)	L_j (10^{49} erg s $^{-1}$)	Ref
191221B	1.148	13	0.0454	36	9.4	7.73	18
200826A*	0.7481	0.65	0.24	0.717	6	520.26	19
200829A	1.25	6.9	0.09	141	44.668	245.20	20
201015A	0.423	10	0.9772	0.011	1.6218	110.94	21
201216C	1.1	48	0.123	57.6	1122	390.38	21
210104A	0.46	35	1.0	1.3	0.39	35.25	22
210204A*	0.876	207	0.024	114.8	114.82	0.60	23
210205A	2.514	22.7	0.96	1.52	2.3988	279.54	24
210731A	1.2525	22.5	$\gtrsim 0.1047$	1.29	63	35.28	25
210905A	6.312	870	0.147	127	508	57.66	26
220101A	4.618	128	0.0229	300	34674	402.49	27
221009A	0.151	327	0.024	1500	676.08	2.21	28

Notes:

* GRBs with SNe observed.

References:

(1) Song, Liu, & Li (2018); (2) Song & Liu (2019); (3) Kangas & Fruchter (2021); (4) Wang et al. (2018); (5) Li et al. (2018); (6) Lü et al. (2018); (7) Yi et al. (2017); (8) Tanvir et al. (2018); (9) Li et al. (2020); (10) Xin et al. (2018); (11) Marongiu et al. (2022); (12) Han et al. (2022); (13) Laskar et al. (2019); (14) Zhu et al. (2023); (15) Sharma, Iyyani, & Bhattacharya (2021); (16) Liu et al. (2022); (17) Sato et al. (2021); (18) Urata et al. (2023); (19) Ahumada et al. (2021); (20) Li et al. (2023); (21) Zhang et al. (2023); (22) Zhang et al. (2022); (23) Kumar et al. (2022); (24) Gupta et al. (2022); (25) de Wet et al. (2023); (26) Rossi et al. (2022); (27) Mei et al. (2022); (28) Ren et al. (2023).

Table 2. ULGRB Data

GRB	z	T_{90} (s)	θ_j (rad)	$E_{\gamma,iso}$ (10^{52} erg)	$E_{k,iso}$ (10^{52} erg)	L_j (10^{49} erg s $^{-1}$)	Ref
060218A*	0.0331	2100	$\gtrsim 1.4$	0.0062	0.0001	0.0030	1
091024	1.092	1020	> 0.071	28	37.2529	0.34	2
100316D*	0.0591	1300	> 1.3963	0.006	0.000605	0.0052	3
101225A	0.847	1090	0.2094	10	24	1.2631	4
111209A*	0.677	15000	> 0.2094	96	59	0.3799	4
121027A	1.773	1070	0.2094	140	15	8.8069	4
130925A	0.35	4500	0.0012	15	22.779	8.46E-06	5,6

References:

(1) Soderberg et al. (2006); (2) Song, Liu, & Li (2018); (3) Margutti et al. (2013); (4) Nakauchi et al. (2013); (5) Evans et al. (2014); (6) Horesh et al. (2015).

should weaken the domination of the neutrino annihilation process to power GRBs.

ACKNOWLEDGEMENTS

We thank Hui-Min Qu, Shuang-Xi Yi, Shu-Jin Hou, Shu-Yu Hu, and Cui-Ying Song for the helpful discussion. This work was supported by the National Natural Science Foundation of China under grants 12173031 and 12221003.

DATA AVAILABILITY

The data underlying this article will be shared on reasonable request to the first author.

REFERENCES

Abbott B. P., Abbott R., Abbott T. D., Acernese F., Ackley K., Adams C., Adams T., et al., 2017, *PhRvL*, 119, 161101. doi:10.1103/PhysRevLett.119.161101

Abbott R., Abbott T. D., Abraham S., Acernese F., Ackley K., Adams A., Adams C., et al., 2021, *ApJL*, 915, L5. doi:10.3847/2041-8213/ac082e

Ahumada T., Singer L. P., Anand S., Coughlin M. W., Kasliwal M. M., Ryan G., Andreoni I., et al., 2021, *NatAs*, 5, 917. doi:10.1038/s41550-021-01428-7

Bardeen J. M., Press W. H., Teukolsky S. A., 1972, *ApJ*, 178, 347. doi:10.1086/151796

Becerra R. L., Dichiara S., Watson A. M., Troja E., Fraija N., Klotz A., Butler N. R., et al., 2019, *ApJ*, 881, 12. doi:10.3847/1538-4357/ab275b

Belczynski K., Kalogera V., Rasio F. A., Taam R. E., Zezas A., Bulik T., Maccarone T. J., et al., 2008, *ApJS*, 174, 223. doi:10.1086/521026

Berger E., Chornock R., Holmes T. R., Foley R. J., Cucchiara A., Wolf C., Podsiadlowski P., et al., 2011, *ApJ*, 743, 204. doi:10.1088/0004-637X/743/2/204

Blandford R. D., Znajek R. L., 1977, *MNRAS*, 179, 433. doi:10.1093/mnras/179.3.433

Burrows D. N., Hill J. E., Nousek J. A., Kennea J. A., Wells A., Osborne J. P., Abbey A. F., et al., 2005, *SSRv*, 120, 165. doi:10.1007/s11214-005-5097-2

Burrows D. N., Romano P., Falcone A., Kobayashi S., Zhang B., Moretti A., O’Brien P. T., et al., 2005, *Sci*, 309, 1833. doi:10.1126/science.1116168

Table 3. SGRB Data

GRB	z	T_{90} (s)	θ_j (rad)	$E_{\gamma,iso}$ (10^{52} erg)	$E_{k,iso}$ (10^{52} erg)	L_j (10^{49} erg s $^{-1}$)	Ref
050509B	0.225	0.04	>0.05	0.00024	0.0055	0.22	1
050709	0.161	0.07	>0.26	0.0027	0.0016	2.41	1
050724A	0.257	3	>0.35	0.009	0.027	0.92	1
051210	1.3	1.3	>0.05	0.4	0.238	1.41	1
051221A	0.5465	1.4	0.12	0.28	1.26	12.25	1
060502B	0.287	0.09	>0.05	0.003	0.012	0.27	1
060801	1.13	0.5	0.056	0.7	0.071	5.17	1
061006	0.438	0.4	0.41	3	0.314	986.76	1
061201	0.111	0.8	0.017	3	0.007	0.60	1
061210	0.409	0.2	>0.37	0.09	0.086	84.87	1
070429B	0.902	0.5	>0.05	0.07	0.451	2.48	1
070714B	0.923	2.0	0.33	1.16	0.232	72.88	1
070724A	0.457	0.4	0.27	0.003	0.099	13.54	1
070729	0.8	0.9	>0.05	0.017	0.132	0.37	1
070809	0.473	1.3	0.4	0.0056	0.391	35.95	1
071227	0.381	1.8	>0.026	0.1	0.025	0.03	1
080905A	0.122	1.0	0.28	0.0005	0.0024	0.13	1
090426	2.609	1.2	0.07	0.5	13.5	103.16	1
090510	0.903	0.3	0.017	4.47	0.307	4.38	1
090515	0.403	0.04	>0.05	0.0008	0.062	2.75	1
100117A	0.92	0.3	0.27	0.09	0.11	46.66	1
100206A	0.408	0.1	>0.05	0.0763	0.0073	1.47	1
100625A	0.453	0.3	>0.05	0.075	0.0093	0.51	1
101219A	0.718	0.6	0.29	0.49	0.045	64.42	1
110731A	2.83	7.3	>0.15	68	7.5	472.06	2
111020A	1.5	0.4	0.05~0.14	0.19	1.2	11.91	3
111117A	1.3	0.5	0.11	0.338	0.377	18.13	1
120804A	1.3	0.81	>0.19	0.7	0.7	71.75	1
130603B	0.356	0.18	0.07	0.212	0.28	9.08	1
131001A	0.717	1.54	>0.05	0.037	0.541	0.81	1
140622A	0.959	0.13	>0.05	0.0065	0.977	18.53	1
140903A	0.351	0.3	0.09	0.006	4.3	78.53	4
150101B	0.1343	0.012	\gtrsim 0.16	0.0013	0.61	712.15	5
160624A	0.483	0.2	0.16	0.047	0.05	9.11	6
160821B	0.16	0.48	0.063	0.021	8	38.47	1
170817A	0.009783	0.5	0.2	0.0022	0.02	0.90	7
180418A	0.5	1.504	>0.122	0.3	0.077	2.80	8
181123B	1.754	0.26	1.57	0.026	0.234	3394.17	9
200522A	0.5536	0.62	0.25	0.0084	0.015849	1.97	10
200826A*	0.7481	1.14	0.24	0.717	6	296.64	11
211211A	0.076	6	0.033	0.76	1.2882	0.20	12

Notes:

GRB 200826A is a short LGRB, which is associated with SNe.

References:

(1) Song, Liu, & Li (2018); (2) Lü et al. (2017); (3) Fong et al. (2012); (4) Troja et al. (2016); (5) Fong et al. (2016); (6) O'Connor et al. (2021); (7) Murase et al. (2018); (8) Becerra et al. (2019); (9) Dichiaro et al. (2021); (10) Fong et al. (2021); (11) Ahumada et al. (2021); (12) Zhong, Li, & Dai (2023).

Dai Z. G., Lu T., 1998a, A&A, 333, L87.
doi:10.48550/arXiv.astro-ph/9810402

Dai Z. G., Lu T., 1998b, PhRvL, 81, 4301.
doi:10.1103/PhysRevLett.81.4301

de Wet S., Laskar T., Groot P. J., Cavallaro F., Nicuesa Guelbenzu A., Chastain S., Izzo L., et al., 2023, A&A, 671, A116.
doi:10.1051/0004-6361/202244917

Dichiaro S., Troja E., Beniamini P., O'Connor B., Moss M., Lien A. Y., Ricci R., et al., 2021, ApJL, 911, L28. doi:10.3847/2041-8213/abf562

Du M., Yi S.-X., Liu T., Song C.-Y., Xie W., 2021, ApJ, 908, 242.
doi:10.3847/1538-4357/abd6bd

Duncan R. C., Thompson C., 1992, ApJL, 392, L9.
doi:10.1086/186413

Eichler D., Livio M., Piran T., Schramm D. N., 1989, Natur, 340,

126. doi:10.1038/340126a0

Evans P. A., Willingale R., Osborne J. P., O'Brien P. T., Tanvir N. R., Frederiks D. D., Pal'shin V. D., et al., 2014, MNRAS, 444, 250. doi:10.1093/mnras/stu1459

Fan Y.-Z., Wei D.-M., 2011, ApJ, 739, 47. doi:10.1088/0004-637X/739/1/47

Fan Y.-Z., Xu D., 2006, MNRAS, 372, L19. doi:10.1111/j.1745-3933.2006.00217.x

Fong W., Berger E., Margutti R., Zauderer B. A., Troja E., Czekala I., Chornock R., et al., 2012, ApJ, 756, 189.
doi:10.1088/0004-637X/756/2/189

Fong W., Margutti R., Chornock R., Berger E., Shappee B. J., Levan A. J., Tanvir N. R., et al., 2016, ApJ, 833, 151.
doi:10.3847/1538-4357/833/2/151

Fong W., Laskar T., Rastinejad J., Escorial A. R., Schroeder

- G., Barnes J., Kilpatrick C. D., et al., 2021, *ApJ*, 906, 127. doi:10.3847/1538-4357/abc74a
- Gammie C. F., Shapiro S. L., McKinney J. C., 2004, *ApJ*, 602, 312. doi:10.1086/380996
- Gehrels N., Chincarini G., Giommi P., Mason K. O., Nousek J. A., Wells A. A., White N. E., et al., 2004, *ApJ*, 611, 1005. doi:10.1086/422091
- Gendre B., Stratta G., Atteia J. L., Basa S., Boër M., Coward D. M., Cutini S., et al., 2013, *ApJ*, 766, 30. doi:10.1088/0004-637X/766/1/30
- Greiner J., Mazzali P. A., Kann D. A., Krühler T., Pian E., Prentice S., Olivares E. F., et al., 2015, *Natur*, 523, 189. doi:10.1038/nature14579
- Gupta R., Kumar A., Pandey S. B., Castro-Tirado A. J., Ghosh A., Dimple H., Fernández-García E., et al., 2022, *JApA*, 43, 11. doi:10.1007/s12036-021-09794-4
- Han S., Li X., Jiang L., Jin Z., He H., Wang Y., Wei D., 2022, *Univ*, 8, 248. doi:10.3390/universe8040248
- Hjorth J., Sollerman J., Møller P., Fynbo J. P. U., Woosley S. E., Kouveliotou C., Tanvir N. R., et al., 2003, *Natur*, 423, 847. doi:10.1038/nature01750
- Horesh A., Cenko S. B., Perley D. A., Kulkarni S. R., Hal-linan G., Bellm E., 2015, *ApJ*, 812, 86. doi:10.1088/0004-637X/812/1/86
- Huang B.-Q., Liu T., 2021, *ApJ*, 916, 71. doi:10.3847/1538-4357/ac07a0
- Janiuk A., Moderski R., Proga D., 2008, *ApJ*, 687, 433. doi:10.1086/591841
- Kamble A., Misra K., Bhattacharya D., Sagar R., 2009, *MNRAS*, 394, 214. doi:10.1111/j.1365-2966.2008.13504.x
- Kangas T., Fruchter A. S., 2021, *ApJ*, 911, 14. doi:10.3847/1538-4357/abe76b
- Kato S., Fukue J., Mineshige S., 2008, *bhad.book*
- Kawanaka N., Piran T., Krolik J. H., 2013, *ApJ*, 766, 31. doi:10.1088/0004-637X/766/1/31
- Kouveliotou C., Meegan C. A., Fishman G. J., Bhat N. P., Briggs M. S., Koshut T. M., Paciesas W. S., et al., 1993, *ApJL*, 413, L101. doi:10.1086/186969
- Kumar H., Gupta R., Saraogi D., Ahumada T., Andreoni I., Anupama G. C., Aryan A., et al., 2022, *MNRAS*, 513, 2777. doi:10.1093/mnras/stac1061
- Laskar T., van Eerten H., Schady P., Mundell C. G., Alexander K. D., Barniol Duran R., Berger E., et al., 2019, *ApJ*, 884, 121. doi:10.3847/1538-4357/ab40ce
- Lee H. K., Kim H.-K., 2000, *JKPS*, 36, 188. doi:10.48550/arXiv.astro-ph/0008360
- Lee H. K., Wijers R. A. M. J., Brown G. E., 2000, *PhR*, 325, 83. doi:10.1016/S0370-1573(99)00084-8
- Levan A. J., Tanvir N. R., Starling R. L. C., Wiersema K., Page K. L., Perley D. A., Schulze S., et al., 2014, *ApJ*, 781, 13. doi:10.1088/0004-637X/781/1/13
- Li J., Lin D.-B., Lu R.-J., Jiang L.-Y., Liang W.-Q., Chen Z.-L., Li X.-Y., et al., 2023, *ApJ*, 944, 21. doi:10.3847/1538-4357/acaf68
- Li L., Wu X.-F., Lei W.-H., Dai Z.-G., Liang E.-W., Ryde F., 2018, *ApJS*, 236, 26. doi:10.3847/1538-4365/aabaf3
- Li L., Wang X.-G., Zheng W., Pozanenko A. S., Filippenko A. V., Qin S., Wang S.-Q., et al., 2020, *ApJ*, 900, 176. doi:10.3847/1538-4357/aba757
- Liu H.-Y., Wang X.-G., Xin L.-P., Zhou Z.-M., Chen L.-J., Li B., Yang Y.-G., et al., 2022, *RAA*, 22, 065002. doi:10.1088/1674-4527/ac65e6
- Liu T., Gu W.-M., Xue L., Lu J.-F., 2007, *ApJ*, 661, 1025. doi:10.1086/513689
- Liu T., Gu W.-M., Zhang B., 2017, *NewAR*, 79, 1. doi:10.1016/j.newar.2017.07.001
- Liu T., Hou S.-J., Xue L., Gu W.-M., 2015a, *ApJS*, 218, 12. doi:10.1088/0067-0049/218/1/12
- Liu T., Lin Y.-Q., Hou S.-J., Gu W.-M., 2015b, *ApJ*, 806, 58. doi:10.1088/0004-637X/806/1/58
- Liu T., Song C.-Y., Zhang B., Gu W.-M., Heger A., 2018, *ApJ*, 852, 20. doi:10.3847/1538-4357/aa9e4f
- Liu T., Wei Y.-F., Xue L., Sun M.-Y., 2021, *ApJ*, 908, 106. doi:10.3847/1538-4357/abd24e
- Luo Y., Gu W.-M., Liu T., Lu J.-F., 2013, *ApJ*, 773, 142. doi:10.1088/0004-637X/773/2/142
- Lü H.-J., Lan L., Zhang B., Liang E.-W., Kann D. A., Du S.-S., Shen J., 2018, *ApJ*, 862, 130. doi:10.3847/1538-4357/aacd03
- Lü H., Wang X., Lu R., Lan L., Gao H., Liang E., Graham M. L., et al., 2017, *ApJ*, 843, 114. doi:10.3847/1538-4357/aa78f0
- MacFadyen A. I., Woosley S. E., 1999, *ApJ*, 524, 262. doi:10.1086/307790
- Malesani D., Tagliaferri G., Chincarini G., Covino S., Della Valle M., Fugazza D., Mazzali P. A., et al., 2004, *ApJL*, 609, L5. doi:10.1086/422684
- Margutti R., Soderberg A. M., Wieringa M. H., Edwards P. G., Chevalier R. A., Morsony B. J., Barniol Duran R., et al., 2013, *ApJ*, 778, 18. doi:10.1088/0004-637X/778/1/18
- Marongiu M., Guidorzi C., Stratta G., Gomboc A., Jordana-Mitjans N., Dichiaro S., Kobayashi S., et al., 2022, *A&A*, 658, A11. doi:10.1051/0004-6361/202140403
- Mei A., Oganesyan G., Tsvetkova A., Ravasio M. E., Banerjee B., Brighenti F., Ronchini S., et al., 2022, *ApJ*, 941, 82. doi:10.3847/1538-4357/aca091
- Mészáros P., Rees M. J., 1993, *ApJ*, 405, 278. doi:10.1086/172360
- Metzger B. D., 2019, *LRR*, 23, 1. doi:10.1007/s41114-019-0024-0
- Metzger B. D., Giannios D., Thompson T. A., Bucciantini N., Quataert E., 2011, *MNRAS*, 413, 2031. doi:10.1111/j.1365-2966.2011.18280.x
- Murase K., Toomey M. W., Fang K., Oikonomou F., Kimura S. S., Hotokezaka K., Kashiyama K., et al., 2018, *ApJ*, 854, 60. doi:10.3847/1538-4357/aaa48a
- Murguia-Berthier A., Ramirez-Ruiz E., De Colle F., Janiuk A., Rosswog S., Lee W. H., 2021, *ApJ*, 908, 152. doi:10.3847/1538-4357/abd08e
- Nakar E., 2007, *PhR*, 442, 166. doi:10.1016/j.physrep.2007.02.005
- Nakauchi D., Kashiyama K., Suwa Y., Nakamura T., 2013, *ApJ*, 778, 67. doi:10.1088/0004-637X/778/1/67
- Narayan R., Paczyński B., Piran T., 1992, *ApJL*, 395, L83. doi:10.1086/186493
- Novikov I. D., 1998, *GrCo*, 4, 135
- O'Connor B., Troja E., Dichiaro S., Chase E. A., Ryan G., Cenko S. B., Fryer C. L., et al., 2021, *MNRAS*, 502, 1279. doi:10.1093/mnras/stab132
- Paczyński B., 1991, *AcA*, 41, 257
- Paczyński B., 1998, *ApJL*, 494, L45. doi:10.1086/311148
- Perna R., Lazzati D., Cantiello M., 2018, *ApJ*, 859, 48. doi:10.3847/1538-4357/aabcc1
- Popham R., Woosley S. E., Fryer C., 1999, *ApJ*, 518, 356. doi:10.1086/307259
- Qi Y.-Q., Liu T., Huang B.-Q., Wei Y.-F., Bu D.-F., 2022, *ApJ*, 925, 43. doi:10.3847/1538-4357/ac3757
- Qu H.-M., Liu T., 2022, *ApJ*, 929, 83. doi:10.3847/1538-4357/ac5f4b
- Rees M. J., Mészáros P., 1992, *MNRAS*, 258, 41. doi:10.1093/mnras/258.1.41P
- Ren J., Wang Y., Zhang L.-L., Dai Z.-G., 2023, *ApJ*, 947, 53. doi:10.3847/1538-4357/acc57d
- Rossi A., Frederiks D. D., Kann D. A., De Pasquale M., Pian E., Lamb G., D'Avanzo P., et al., 2022, *A&A*, 665, A125. doi:10.1051/0004-6361/202243225
- Rosswog S., Ramirez-Ruiz E., Davies M. B., 2003, *MNRAS*, 345, 1077. doi:10.1046/j.1365-2966.2003.07032.x
- Ruffert M., Janka H.-T., Takahashi K., Schaefer G., 1997, *A&A*, 319, 122. doi:10.48550/arXiv.astro-ph/9606181
- Sato Y., Obayashi K., Yamazaki R., Murase K., Ohira Y., 2021,

- MNRAS, 504, 5647. doi:10.1093/mnras/stab1273
- Sharma V., Iyyani S., Bhattacharya D., 2021, ApJL, 908, L2. doi:10.3847/2041-8213/abd53f
- Soderberg A. M., Kulkarni S. R., Nakar E., Berger E., Cameron P. B., Fox D. B., Frail D., et al., 2006, Natur, 442, 1014. doi:10.1038/nature05087
- Song C.-Y., Liu T., Gu W.-M., Hou S.-J., Tian J.-X., Lu J.-F., 2015, ApJ, 815, 54. doi:10.1088/0004-637X/815/1/54
- Song C.-Y., Liu T., 2019, ApJ, 871, 117. doi:10.3847/1538-4357/aaf6ae
- Song C.-Y., Liu T., Li A., 2018, MNRAS, 477, 2173. doi:10.1093/mnras/sty783
- Stanek K. Z., Matheson T., Garnavich P. M., Martini P., Berlind P., Caldwell N., Challis P., et al., 2003, ApJL, 591, L17. doi:10.1086/376976
- Surman R., McLaughlin G. C., Hix W. R., 2006, ApJ, 643, 1057. doi:10.1086/501116
- Tanvir N. R., Laskar T., Levan A. J., Perley D. A., Zabl J., Fynbo J. P. U., Rhoads J., et al., 2018, ApJ, 865, 107. doi:10.3847/1538-4357/aadba9
- Troja E., Sakamoto T., Cenko S. B., Lien A., Gehrels N., Castro-Tirado A. J., Ricci R., et al., 2016, ApJ, 827, 102. doi:10.3847/0004-637X/827/2/102
- Urata Y., Toma K., Covino S., Wiersema K., Huang K., Shimoda J., Kuwata A., et al., 2023, NatAs, 7, 80. doi:10.1038/s41550-022-01832-7
- Usov V. V., 1992, Natur, 357, 472. doi:10.1038/357472a0
- Virgili F. J., Mundell C. G., Pal'shin V., Guidorzi C., Margutti R., Melandri A., Harrison R., et al., 2013, ApJ, 778, 54. doi:10.1088/0004-637X/778/1/54
- Wang X.-G., Zhang B., Liang E.-W., Lu R.-J., Lin D.-B., Li J., Li L., 2018, ApJ, 859, 160. doi:10.3847/1538-4357/aabc13
- Wei Y.-F., Liu T., Xue L., 2021, MNRAS, 507, 431. doi:10.1093/mnras/stab2153
- Woosley S. E., 1993, ApJ, 405, 273. doi:10.1086/172359
- Xin L.-P., Zhong S.-Q., Liang E.-W., Wang J., Liu H., Zhang T.-M., Huang X.-L., et al., 2018, ApJ, 860, 8. doi:10.3847/1538-4357/aabf3d
- Yi S.-X., Lei W.-H., Zhang B., Dai Z.-G., Wu X.-F., Liang E.-W., 2017, JHEAp, 13, 1. doi:10.1016/j.jheap.2017.01.001
- Zalamea I., Beloborodov A. M., 2011, MNRAS, 410, 2302. doi:10.1111/j.1365-2966.2010.17600.x
- Zhang B., 2006, Natur, 444, 1010. doi:10.1038/4441010a
- Zhang B., Fan Y. Z., Dyks J., Kobayashi S., Mészáros P., Burrows D. N., Nousek J. A., et al., 2006, ApJ, 642, 354. doi:10.1086/500723
- Zhang B., Liang E., Page K. L., Grupe D., Zhang B.-B., Barthelmy S. D., Burrows D. N., et al., 2007b, ApJ, 655, 989. doi:10.1086/510110
- Zhang B., Zhang B.-B., Liang E.-W., Gehrels N., Burrows D. N., Mészáros P., 2007a, ApJL, 655, L25. doi:10.1086/511781
- Zhang B., Zhang B.-B., Virgili F. J., Liang E.-W., Kann D. A., Wu X.-F., Proga D., et al., 2009, ApJ, 703, 1696. doi:10.1088/0004-637X/703/2/1696
- Zhang B.-B., Zhang B., Murase K., Connaughton V., Briggs M. S., 2014, ApJ, 787, 66. doi:10.1088/0004-637X/787/1/66
- Zhang L.-L., Ren J., Wang Y., Liang E.-W., 2023, ApJ, 952, 127. doi:10.3847/1538-4357/acd190
- Zhang L.-L., Xin L.-P., Wang J., Han X.-H., Xu D., Zhu Z.-P., Wu C., et al., 2022, ApJ, 941, 63. doi:10.3847/1538-4357/aca08f
- Zhong S.-Q., Li L., Dai Z.-G., 2023, ApJL, 947, L21. doi:10.3847/2041-8213/acca83
- Zhu Z.-P., Xu D., Fynbo J. P. U., Fu S.-Y., Zhang J.-B., Liu X., Jiang S.-Q., et al., 2023, ApJ, 948, 30. doi:10.3847/1538-4357/acbd96